Late Gadolinium Enhancement Cardiac Magnetic Resonance Tissue Characterization for Cancer-Associated Cardiac Masses: Metabolic and Prognostic Manifestations in Relation to Whole-Body Positron Emission Tomography

Angel T. Chan, MD, PhD; Josef Fox, MD; Rocio Perez Johnston, MD; Jiwon Kim, MD; Lillian R. Brouwer, BA; John Grizzard, MD; Raymond J. Kim, MD; Mathew Matasar, MD; Jinru Shia, MD; Chaya S. Moskowitz, PhD; Richard Steingart, MD; Jonathan W. Weinsaft, MD

Background—Cardiac magnetic resonance (CMR) differentiates neoplasm from thrombus via contrast enhancement; positron emission tomography (PET) assesses metabolism. The relationship between CMR contrast enhancement and metabolism on PET is unknown.

Methods and Results—The population included 121 cancer patients undergoing CMR and ^{18}F-fluorodeoxyglucose (^{18}F-FDG)–PET, including 66 with cardiac masses and cancer-matched controls. Cardiac mass etiology (neoplasm, thrombus) on CMR was defined by late gadolinium enhancement; PET was read blinded to CMR for diagnostic performance, then colocalized to measure FDG avidity. Of CMR-evidenced thrombi (all nonenhancing), none were detected by PET. For neoplasm, PET yielded reasonable sensitivity (70–83%) and specificity (75–88%). Lesions undetected by PET were more likely to be highly mobile ($P=0.001$) despite similar size ($P=0.33$). Among nonmobile neoplasms, PET sensitivity varied in relation to extent of CMR-evidenced avascularity; detection of diffusely enhancing or mixed lesions was higher versus predominantly avascular neoplasms (87% versus 63%). Colocalized analyses demonstrated 2- to 4-fold higher FDG uptake in neoplasm versus thrombus ($P<0.001$); FDG uptake decreased stepwise when neoplasms were partitioned based on extent of avascularity on late gadolinium enhancement CMR ($P\leq0.001$). Among patients with neoplasm, signal-to-noise ratio on late gadolinium enhancement CMR moderately correlated with standardized uptake values on PET ($r=0.42–0.49$, $P<0.05$). Mortality was higher among patients with CMR-evidenced neoplasm versus controls (hazard ratio: 1.99 [95% CI, 1.1–3.6]; $P=0.03$) despite nonsignificant differences when partitioned via FDG avidity (hazard ratio: 1.56 [95% CI, 0.85–2.74]; $P=0.16$). Among FDG-positive neoplasms detected concordantly with CMR, mortality risk versus cancer-matched controls was equivalently increased (hazard ratio: 2.12 [95% CI, 1.01–4.44]; $P=0.047$).

Conclusions—CMR contrast enhancement provides a criterion for neoplasm that parallels FDG-evidenced metabolic activity and stratifies prognosis. Extent of tissue avascularity on late gadolinium enhancement CMR affects cardiac mass identification by FDG-PET. (*J Am Heart Assoc.* 2019;8:e011709. DOI: 10.1161/JAHA.118.011709.)

Key Words: cardiac magnetic resonance • cardiac neoplasm • cardio–oncology • positron emission tomography

Cardiac masses—including neoplasm and thrombus—impact therapeutic management, including decision-making regarding anticancer regimen and anticoagulation. Imaging is widely used to screen for neoplasm and thrombus, but differentiation between the 2 based on morphology alone can be challenging given similarities in size and shape. Tissue characterization is known to improve diagnosis of cardiac masses over morphological imaging, but a variety of approaches have been used for this purpose.[1–8] Given the need to reliably identify and differentiate cardiac masses,

Clinical Perspective

What Is New?

- This study is the first to test tissue characterization of cardiac masses by cardiac magnetic resonance with late gadolinium enhancement (LGE-CMR) in relation to metabolic activity on positron emission tomography (PET).
- Among a broad cancer cohort, identification of CMR-evidenced cardiac masses by fluorodeoxyglucose–PET varied in relation to avascular tissue composition on LGE-CMR, as shown by a lack of detection of thrombi (all nonenhancing) and lower detection rates for predominantly avascular neoplasms.
- Among patients with CMR-evidenced cardiac neoplasms, fluorodeoxyglucose avidity on PET correlated with magnitude of contrast enhancement and the improved detection of cardiac neoplasms by LGE-CMR compared with PET corresponded to incremental risk stratification for all-cause mortality.

What Are the Clinical Implications?

- Findings of this study indicate that CMR-evidenced contrast enhancement provides a criterion for cardiac neoplasm that affects PET diagnostic detection, parallels metabolic activity, and stratifies prognosis.
- Extent of tissue avascularity on LGE-CMR affects cardiac mass identification by fluorodeoxyglucose–PET.
- Whereas contrast-enhancing and FDG-avid cardiac lesions portend similarly poor prognosis, augmented neoplasm detection of avascular and/or highly mobile neoplasms by CMR results in improved prognostic risk stratification.

effective clinical management of cancer patients is predicated on optimal imaging strategies for this purpose.

Cardiac magnetic resonance (CMR) has been well validated for detection and differentiation of neoplasm and thrombus.[1,3,5–9] Using the technique of late gadolinium enhancement (LGE), neoplasm and thrombus can be identified based on differential tissue properties stemming from presence or absence of vascular supply. Lack of enhancement has been shown to yield incremental utility as a diagnostic criterion for thrombus that stratifies mortality and embolic event risk.[1,6–8,10] Paralleling the fact that tumor genesis relies on vascular supply, recent data from our group have shown contrast enhancement to be a criterion for neoplasm that agrees with histopathology and predicts prognosis.[1,3]

Tissue characterization imaging can also be provided via alternative approaches, such as assessment of metabolic (glycolytic) activity via ^{18}F-fluorodeoxyglucose (^{18}F-FDG) positron emission tomography (PET). FDG-PET is typically performed for "whole-body" imaging of cancer patients, so as to comprehensively assess disease burden—including extent of affected organs. In the context of whole-body imaging, masses or neoplasms involving the heart may be detected, just as they may be detected elsewhere in the body. Moreover, whereas CMR requires specialized equipment, PET is available in nearly all cancer centers—fostering its appeal as a screening tool. Utility of whole-body PET in relation to LGE-CMR for assessment of cardiac masses has yet to be tested. In addition, whereas thrombus is uniformly avascular (nonenhancing) and neoplasm can include avascular components, it is unknown whether this tissue property is a marker of metabolic activity that affects detection by PET.

Aims of the current study were (1) to determine whether differences in CMR-evidenced contrast enhancement between neoplasm and thrombus parallel differential metabolism on PET; (2) to identify factors affecting performance of visual and quantitative PET in relation to the reference of CMR; and (3) to assess whether differential detection of cardiac masses by CMR and PET affects their relative utility for prognostic risk stratification.

Methods

The data, analytic methods, and study materials will be made available to other researchers for purposes of reproducing the results or replicating the procedure, on request (contingent on approval of the Memorial Sloan Kettering Cancer Center institutional review board and assurance of data deidentification).

Study Population

The population included consecutive adults (≥18 years old) with solid tumors and cardiac masses who underwent CMR and routine whole-body ^{18}F-FDG–PET within a 3-month interval: cardiac masses were identified using the reference
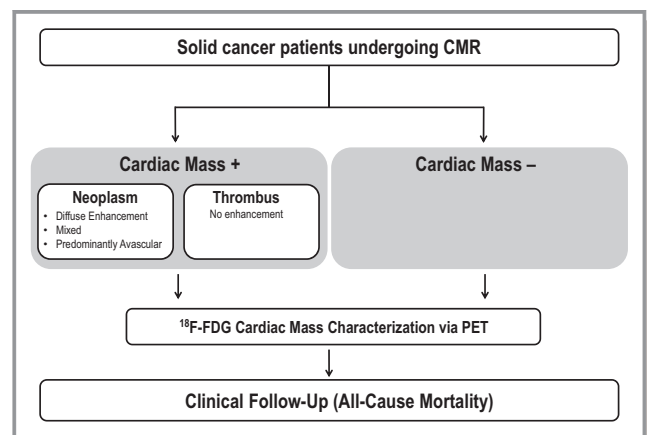
Figure 1. Study design, inclusive of cardiac mass assessment via late gadolinium enhancement CMR (LGE-CMR; for contrast enhancement), ^{18}F–fluorodeoxyglucose (^{18}F-FDG)–positron emission tomography (PET; for metabolic activity) and subsequent clinical follow-up (for all-cause mortality).

of CMR, for which a cardiac mass was defined via established criteria as a discrete tissue prominence independent from chamber cavity or normal anatomic structures.[1,3,5–8] Patients with cardiac masses were matched (1:1) to patients without cardiac masses on CMR but equivalent primary cancer diagnosis and disease stage; each cardiac mass subgroup (neoplasm, thrombus) was matched to distinct (cardiac mass–negative) controls without overlap between controls in respective subgroups.

Figure 1 provides a schematic of the research protocol. Clinical data were collected in a standardized manner, including cancer diagnosis/stage and anticancer therapies administered within 6 months of imaging. Mortality was assessed to test prognosis in relation to the presence of a cardiac mass as identified by CMR and PET. Patient characterization was performed in the context of an ongoing registry of cancer-associated cardiac masses, for which 42% of the current population was included in our prior studies testing prognostic implications of neoplasm and thrombus identified by CMR.[1,3]

This study entailed analysis of imaging and ancillary data acquired for clinical purposes between 2012 and 2018; no dedicated interventions (imaging or otherwise) were performed exclusively for research purposes. For whole-body PET, all imaging was performed for the indication of general cancer (extent of disease) staging. For CMR, leading clinical indications were for assessment of suspected cardiac masses (70%) or cardiomyopathy (20%). CMR was most commonly prompted by echo findings (65%) and, less commonly, to evaluate findings of other tests (13% PET, 11% computed tomography, 11% no prior imaging).

Ethics approval for this protocol was provided by the Memorial Sloan Kettering Cancer Center institutional review board, which approved a waiver of informed consent for analysis of preexisting clinical data.

Imaging Protocol

Cardiac magnetic resonance

CMR was performed on commercial (1.5-T [95%], 3.0-T [5%]) scanners. Examinations included ECG-gated cine- and LGE components; both were obtained in contiguous left ventricular short-axis (mitral annulus–apex) and long-axis (2, 3, 4 chamber) orientations. Cine-CMR utilized a steady-state free-precession pulse sequence. LGE-CMR utilized an inversion recovery pulse sequence; images were acquired 8 to 30 minutes after gadolinium (0.2 mmol/kg) injection. Conventional (inversion time [TI]: ≈300 ms) and long-TI (600 ms) LGE-CMR were used to discern cardiac mass vascularity concordant with prior methods applied and validated by our group.[1,3,6–8] Conventional LGE-CMR was acquired in all patients; additional breath holds for supplemental long-TI

imaging were tolerated in 95% (63/66) of patients with cardiac masses (100% thrombus, 93% neoplasm).

Positron emission tomography

Whole-body ^{18}F–FDG–PET was performed on commercial scanners (92% on GE Discovery). Consistent with established institutional PET protocols for whole-body cancer surveillance, image acquisition was performed without dedicated cardiac tailoring (ie, neither ECG nor respiratory gating were used). The protocol entailed intravenous injection of ^{18}F-FDG (mean: 459±33 MBq) following at least a 4- to 6-hour fast: To confirm adequate metabolic preparation, blood glucose levels (mean: 99.2±25.2 mg/dL) were checked before ^{18}F-FDG injection. After a target 1-hour uptake period, a low-dose attenuation-correction computed tomography scan (120–140 kV; ≈80 mA) was acquired, followed by acquisition of PET images. PET data were obtained in 3-dimensional mode from the middle thigh to the base of the skull at 3 to 5 minutes per bed position; images were reconstructed using manufacturer-supplied software and reviewed on a commercially available software platform (Advantage Workstation; GE Healthcare).

Image Analysis

Blinded diagnostic interpretation of CMR and PET was performed by designated physicians with expertise in each respective modality (CMR: J.W.W.; PET: J.J.F.) who had previously interpreted ≥10 000 prior exams. A cardiac mass was defined via standard criteria:

Cardiac magnetic resonance

Cardiac mass subtypes were distinguished via LGE-CMR based on contrast-enhanced tissue properties, in accordance with established criteria previously validated by our group and others[1,3,5–8]:

- *Thrombus* was defined as a cardiac mass with avascular tissue properties based on uniform absence of contrast enhancement.[5–8]
- *Neoplasm* was defined as a cardiac mass with evidence of vascularity on LGE-CMR, as demonstrated by contrast enhancement.[1,3] Lesions were further classified based on contrast-enhancement pattern, for which 3 categories were assigned: *diffuse enhancement*, *predominantly avascular* (areas of no contrast enhancement*), mixed* (enhancing and nonenhancing components).

Figure 2 provides representative examples of cardiac masses, including thrombus and each neoplasm subtype.

Neoplasm and thrombus were scored in a binary manner (present or absent) and localized based on chamber location (right atrium, right ventricle, left atrium, left ventricle)[11] or pericardial involvement. Quantitative analyses of long-TI LGE–
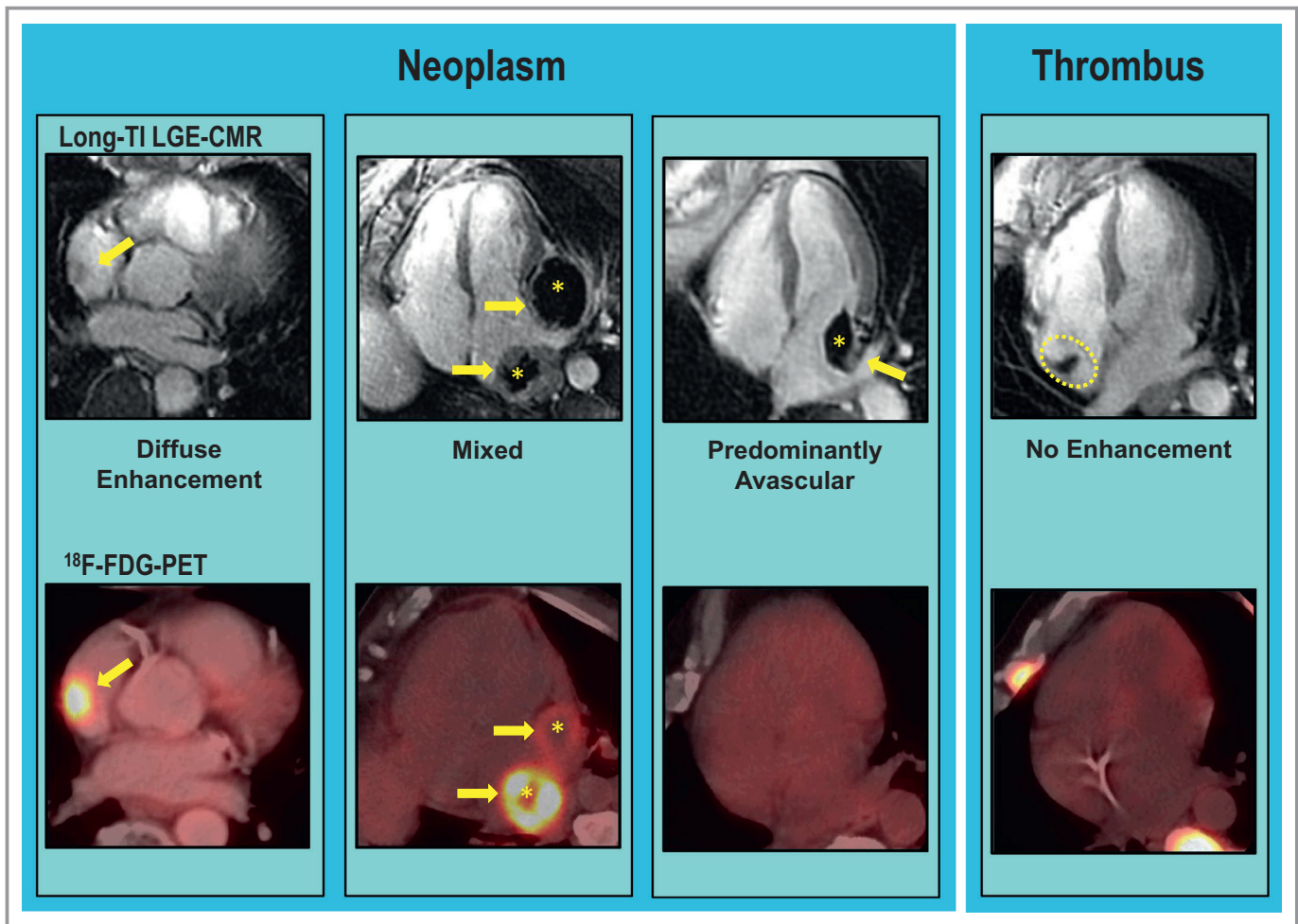
Figure 2. Representative examples of neoplasm and thrombus as established by long inversion time (long-TI) late gadolinium enhancement cardiac magnetic resonance (LGE-CMR) tissue characterization, including neoplasm subtypes comprising diffuse enhancement (left), mixed (prominent enhancing and avascular components; center), and predominantly avascular enhancement (right; arrows indicate contrast-enhancing regions, asterisks indicate avascular regions). Corresponding ^{18}F-fluorodeoxyglucose (^{18}F-FDG)–positron emission tomography (PET) images shown on bottom row: Note prominent FDG avidity corresponding to regions of contrast enhancement, and lack of FDG avidity in both predominantly avascular neoplasm as well as thrombus (far right).

CMR images were used to assess magnitude and pattern of contrast enhancement. For patients with multiple lesions, the largest mass (on long-TI LGE-CMR) was used for quantitative analysis. Concordant with prior methods applied by our group,[1,3] aggregate signal-to-noise ratio (SNR) and contrast-enhancement heterogeneity (CEH) in neoplasm and thrombus were measured in regions of interest on the 2-dimensional slice in which the lesion was most prominently visualized. To assess differential enhancement patterns among neoplasm subtypes, SNR and CEH were measured within visually assessed regions of maximal hyper- and hypoenhancement.

Anatomic and functional properties of lesions were assessed on cine-CMR, including size (area, perimeter, and linear dimensions). Prominent mobility was graded in a binary manner, for which it was defined based on maximum excursion between diastolic and systolic frames. Ancillary analyses included

quantification of cardiac chamber size and function, which were measured in accordance with established methods.[1,3]

Positron emission tomography

A cardiac mass was identified on PET as a discrete lesion with differential FDG uptake from the surrounding blood pool and/or myocardium; increased FDG uptake deemed inconsistent with remodeling processes such as fat or myocardial hypertrophy was considered indicative of neoplasm.[2,4]

Following initial blinded PET interpretation for cardiac masses, repeated (unblinded) analysis was performed to discern whether discrepancies between modalities stemmed from quantitative differences in lesion metabolic activity. To do so, examinations were coregistered with CMR, and standardized uptake value (SUV) was quantified in regions colocalized to CMR-evidenced cardiac masses. Paralleling CMR analysis,

both aggregate (regions of interest encompassing entire lesion) and regional (regions of interest colocalized to areas of hypo- and hyperenhancement) SUV measurements were acquired. FDG indices included maximum and mean SUVs. Myocardial, blood, and hepatic FDG uptake was measured in a standardized manner (target region of interest: 1.5 cm^3) for purpose of normalizing background indices (see Data S1 for additional details regarding methods).

Prognostic Assessment

Electronic medical records were reviewed to assess all-cause mortality status in relation to imaging results (cardiac mass as identified by each modality).

Statistical Analysis

Comparisons between groups with or without cardiac masses and between cardiac mass subtypes (neoplasm versus thrombus) were made using Student t tests (expressed as mean$\pm$SD) for continuous variables and χ^2 or Fisher exact tests for categorical variables: Paired testing (eg, t tests or McNemar tests) was used for matched case–control comparisons. Multiple group comparisons between continuous variables were made using ANOVA. Cardiac mass subtypes were compared using nonparametric (Mann–Whitney U) tests (data reported as median and interquartile range [IQR]). Correlation coefficients (Pearson method) were used to test magnitude of association between CMR and PET indices (eg, SNR, SUV). The Kaplan–Meier method was used to estimate survival; Cox proportional hazards models compared mortality risk between groups. Receiver operating characteristic analysis including area under the curve estimates were used to evaluate overall diagnostic test performance of PET indices (absolute and normalized SUVs), and to derive cutoffs (maximal sensitivity, specificity) for LGE-CMR–evidenced neoplasm. Calculations were performed using SPSS (IBM Corp). A 2-sided $P<0.05$ indicated statistical significance.

Results

Population Characteristics

The study population comprised 121 cancer patients who underwent CMR and ^{18}F-FDG–PET within a 3-month interval (median: 14.8 days [IQR: 3.9–34.5 days]), including patients with cardiac masses established by the reference of CMR as well as controls matched for cancer diagnosis and stage.

Table 1 details population characteristics and comparisons between patients with each cardiac mass type (neoplasm, thrombus) and their respective controls. As shown, cancer

diagnosis varied between the neoplasm and thrombus groups. For neoplasm, lung, sarcoma, and lymphoma were the leading diagnoses. Among patients with thrombus, lymphoma was present in half of cases, followed by sarcoma, gastrointestinal, and breast cancer. Neoplasm and thrombus patients were similar to controls with respect to age, clinical indices, anticancer regimen, as well as cardiac structure and function quantified by CMR (all P values not significant). Regarding anatomical distribution, neoplasm location varied widely (35% left ventricle, 28% left atrium, 35% right ventricle, 41% right atrium, 30% pericardium); 28% of affected patients had multiple lesions located in different cardiac chambers. Nearly all (95%) thrombi were localized to the right atrium (n=1 left ventricle).

Visual Diagnostic Assessment of PET for Cardiac Masses

Blinded visual reads were first used to test PET diagnostic performance for presence and type of CMR-evidenced cardiac masses. For CMR-evidenced thrombus, no cases were detected by PET (sensitivity; 0%), consistent with expected absence of metabolic activity of avascular tissue. As detailed in Table 2, PET identified CMR-evidenced neoplasm in two thirds of cases (sensitivity: 70%). Neoplasms undetected by PET encompassed an array of cancer diagnoses (sarcoma, n=6; gastrointestinal, n=3; lung, n=2; lymphoma, n=1; central nervous system, n=1; endocrine, n=1). Regarding FDG uptake pattern, 25% of the cohort had diffuse left ventricular myocardial FDG uptake: PET sensitivity for CMR-evidenced cardiac neoplasm was slightly lower among patients with, compared with those without, diffuse myocardial FDG uptake (60% versus 72%), although specificity was higher (92% versus 74%). As shown in Table 3, diagnostic performance of PET was similar when restricted to patients without conditions that can potentially confound myocardial FDG uptake (diabetes mellitus, anthracycline therapy). In addition, PET performance was similar between groups partitioned based on median interval between CMR and PET, as well as clinical indications for testing.

Analysis was also performed to assess whether neoplasm location, size, or mobility affected PET performance: Among the 14 patients with neoplasms undetected by PET, location varied (36% left ventricle, 14% left atrium, 36% right ventricle, 36% right atrium, 21% pericardium); 14% had multichamber involvement. Neoplasms undetected by PET were more likely to be graded as highly mobile on cine-CMR than were detected lesions (50% versus 3%, $P=0.001$). Of note, neoplasms detected and undetected by PET were of similar size (area: 11.1$\pm$17.3 versus 7.2$\pm$9.9 cm^2 [$P=0.44$]; maximal diameter: 4.3$\pm$2.9 versus 3.4$\pm$2.4 cm [$P=0.33$]), possibly because large intramyocardial lesions occasionally demonstrated similar or lesser SUV uptake than did left ventricle

Table 1. Population Characteristics

		Neoplasm			Thrombus		
	Overall (n=121)	Positive (n=46)	Negative (n=41)	P Value*	Positive (n=20)	Negative (n=14)	P Value*
Clinical characteristics							
Age, y	54±16	57±16	53±17	0.18	49±17	59±13	0.21
Sex (male)	63% (76)	70% (32)	66% (27)	1.00	55% (11)	43% (6)	1.00
BSA, kg/m^2	1.9±0.2	1.9±0.2	1.9±0.3	0.64	1.8±0.2	1.9±0.2	0.75
Cancer etiologies†							
Lymphoma	28% (34)	17% (8)	20% (8)	…	45% (9)	64% (9)	…
Lung	17% (20)	22% (10)	24% (10)	…	0% (0)	0% (0)	…
Sarcoma	17% (20)	22% (10)	17% (7)	…	15% (3)	0% (0)	…
Gastrointestinal	8% (10)	9% (4)	5% (2)	…	15% (3)	7% (1)	…
Breast	7% (8)	2% (1)	2% (1)	…	15% (3)	21% (3)	…
Skin/melanoma	6% (7)	7% (3)	10% (4)	…	0% (0)	0% (0)	…
Stage IV cancer	96% (116)	100% (46)	100% (41)	…	90% (18)	86% (12)	…
Anticancer regimen							
Chemotherapy							
Alkylating agent	38% (46)	33% (15)	34% (14)	1.00	40% (8)	64% (9)	0.13
Platinum	29% (35)	41% (19)	24% (10)	0.12	15% (3)	21% (3)	1.00
Antimetabolite	34% (41)	37% (17)	27% (11)	0.30	35% (7)	43% (6)	1.00
Anthracycline	30% (36)	28% (13)	29% (12)	1.00	25% (5)	43% (6)	0.63
Mitotic inhibitor	22% (26)	30% (14)	27% (11)	0.55	40% (8)	57% (8)	0.63
Biologic agents	34% (41)	44% (20)	34% (14)	0.61	35% (7)	57% (8)	0.45
Radiation therapy	41% (49)	52% (24)	48% (19)	1.00	40% (8)	36% (5)	1.00
Anticoagulation therapy	13% (16)	36% (5)	7% (1)	0.22	35% (7)	7% (1)	1.00
Coronary artery disease	12% (14)	9% (4)	15% (6)	1.00	10% (2)	14% (2)	1.00
Diabetes mellitus	10% (12)	11% (5)	7% (3)	0.45	5% (1)	21% (3)	…
Cardiac morphology and function							
Left ventricle							
Ejection fraction, %	62±12	65±8	61±15	0.30	64±8	57±15	0.12
End-diastolic volume, mL	124±39	115±32	137±42	0.03	117±45	121±32	1.00
End-systolic volume, mL	48±26	42±17	55±32	0.02	42±20	54±30	0.21
Stroke volume, mL	75±24	74±21	81±26	0.35	75±30	66±17	0.31
Myocardial mass, g	123±50	127±49	121±48	0.98	110±52	137±53	0.30
Right ventricle							
Ejection fraction, %	55±8	54±7	55±9	0.82	55±8	54±8	0.54
End-diastolic volume, mL	134±44	132±38	135±45	0.82	133±60	132±37	0.71
End-systolic volume, mL	62±24	61±21	62±25	0.80	60±30	62±22	1.00
Stroke volume, mL	71±27	68±25	73±29	0.85	73±32	70±21	0.54
Atria							
Left atrial area, cm^2	20±6	19±5	20±6	0.74	20±7	24±7	0.03
Right atrial area, cm^2	18±5	18±5	18±5	0.45	17±6	19±6	0.88

Table 1. Continued

	Overall (n=121)	Neoplasm		P Value*	Thrombus		P Value*
		Positive (n=46)	Negative (n=41)		Positive (n=20)	Negative (n=14)	
PET metabolic indices							
Serum glucose, mg/dL	99±25	101±24	95±25	0.18	99±29	103±26	0.39
FDG dose, MBq	459±33	460±31	463±36	0.69	457±28	448±35	0.85
FDG uptake time, min	69±10	68±8	71±12	0.46	68±8	69±11	0.79

Data are shown as mean±SD or % (n). BSA indicates body surface area; FDG, fluorodeoxyglucose; PET, positron emission tomography.

*Matching not possible in 11 patients (5 neoplasm, 6 thrombus) due to nonequivalent cancer diagnoses among control patients with stage IV cancer undergoing cardiac magnetic resonance: *P* values reflect matched cases and controls.

†Other cancer etiologies: primary cardiac (6%, n=7), endocrine (5%, n=6), genitourinary (4%, n=5), central nervous system (3%, n=4), head/neck (1%, n=1).

myocardium: Figures 3 and 4 (Videos S1 and S2) provide representative examples of highly mobile and intramyocardial neoplasms undetected by PET.

Contrast Enhancement in Relation to Metabolic Activity

Quantitative analysis was then performed to test whether visual diagnostic performance was attributable to differential SUV uptake within CMR-defined cardiac mass subtypes. To do so, PET images were colocalized with CMR in an unblinded fashion, and SUV parameters were then measured within the CMR-evidenced cardiac mass location. Table 4 compares neoplasm and thrombus with respect to metabolic activity on PET. As shown, contrast enhancement on CMR paralleled metabolic differences on PET: Maximum and mean standardized FDG uptake values (SUV) within lesions was 2- to 4-fold higher for neoplasm compared with thrombus; an equivalent magnitude of difference was present regardless of whether analysis was performed using absolute or extracardiac normalized SUV (all *P*<0.001). Figure 5A shows that aggregate SNR within lesions was higher among FDG-positive versus FDG-negative neoplasms and that both groups had higher SNR and CEH than did thrombus (CEH: 10.4±9.8 versus 1.9±1.1 [*P*<0.001]; SNR: 31.5±16.1 versus 12.1±6.4 [*P*<0.001]). As shown in Figure 5B, both mean and maximum SUV moderately correlated with SNR within CMR-quantified neoplasms (*r* values between 0.42 and 0.49, both *P*<0.05).

Further analysis was performed to examine regional FDG uptake in relation to regional contrast-enhancement pattern. As shown in Table 5, mixed lesions (with prominent enhancing and avascular components) had greater overall and maximal FDG uptake than did predominantly avascular lesions (both *P*<0.01), paralleling differences between diffusely enhancing and predominantly avascular lesions (both *P*≤0.001). Consistent with this, PET performance varied in relation to a CMR-evidenced contrast enhancement pattern. Among neoplasms that were not highly mobile, PET detection of diffusely enhancing or mixed lesions was 1.4-fold higher compared with detection of predominantly avascular lesions (87% versus 63%).

Quantitative Diagnostic Assessment of PET for Cardiac Masses

SUV indices were tested to determine whether quantitative cutoffs could be used to augment PET test performance. Figure 6A (left) displays SUV uptake in relation to visual PET reads for neoplasm, as well as among cases of thrombus. As shown, maximum SUV was 4-fold higher within neoplasms visually identified on PET versus cases in which neoplasm was not visually discernable (11.0±6.1 versus 2.4±1.4, *P*<0.001); mean SUV demonstrated a 3-fold difference between groups (5.9±2.4 versus 2.2±1.3, *P*<0.001). Of note, mean and maximum SUV were similar (*P*=0.87 and *P*=0.32) between cases of neoplasm for which PET was visually read as negative

Table 2. Diagnostic Performance of Visual Positron Emission Tomography Interpretation for Cardiac Masses on Cardiac Magnetic Resonance (Overall Population)

	Sensitivity	Specificity	Accuracy	Positive Predictive Value	Negative Predictive Value
Cardiac mass*	49% (32/66)	78% (43/55)	62% (75/121)	73% (32/44)	56% (43/77)
Neoplasm	70% (32/46)	78% (43/55)	74% (75/101)	73% (32/44)	75% (43/57)

Data are shown as percentage (frequency).

*Inclusive of neoplasm and thrombus.

Table 3. Diagnostic Performance of Visual Positron Emission Tomography Interpretation for Cardiac Masses on Cardiac Magnetic Resonance (Excluding Diabetic Patients or Those Receiving Anthracycline–Based Chemotherapy)

|	Sensitivity	Specificity	Accuracy	Positive Predictive Value	Negative Predictive Value
Overall (cardiac mass)*	50% (21/42)	75% (24/32)	61% (45/74)	73% (21/29)	53% (24/45)
Neoplasm	75% (21/28)	75% (24/32)	75% (45/60)	72% (21/29)	77% (24/31)

Data are shown as percentage (frequency).
*Inclusive of neoplasm and thrombus.

and cases of thrombus (all undetected by PET), further supporting the notion that visual test interpretation stemmed from quantitative differences in lesion FDG uptake.

Figure 6B (right) provides superimposed receiver operating characteristic curves for quantitative SUV cutoffs in relation to the reference standard of LGE-CMR–evidenced neoplasm:

As shown, maximum and mean SUV yielded equivalent overall performance (area under the curve: 0.78). Regarding individual parameters, data shown in Table 6 demonstrate that quantitative SUV cutoffs yielded reasonable sensitivity and specificity, which was greatest for maximum SUV normalized for hepatic background (83% and 84%, respectively). Of note,
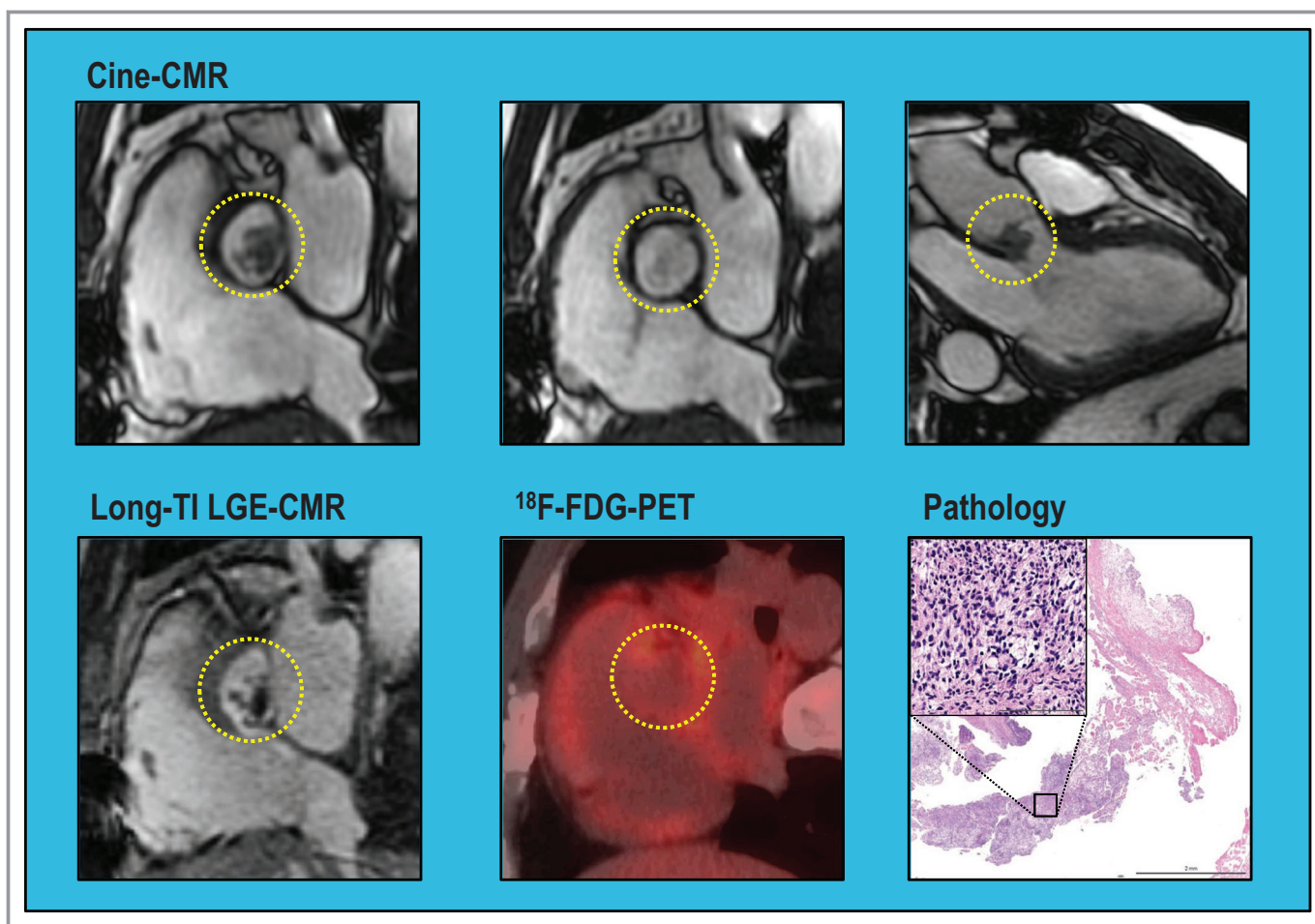
Figure 3. Differential detection of mobile cardiac neoplasm. Mobile neoplasm adherent to the aortic valve in a patient with stage IV sarcoma (lesion denoted within yellow circle). Cine–cardiac magnetic resonance (cine-CMR; top) demonstrates prominent lesion mobility, as shown by migration between systolic and diastolic frames (Video S1). Long inversion time (long-TI) late gadolinium enhancement CMR (LGE-CMR; bottom left) demonstrates a focal aortic lesion with patchy contrast enhancement despite nonvisualization on ^{18}F-fluorodeoxyglucose–positron emission tomography (^{18}F-FDG–PET; bottom center). Pathology data (bottom right) obtained at surgical resection confirmed LGE-CMR diagnosis of neoplasm: note fibrous connective tissue and cellular rich area; high magnification (inset) demonstrates spindle cell morphology, cellular atypia, and nuclear pleomorphism (hematoxylin and eosin stain).
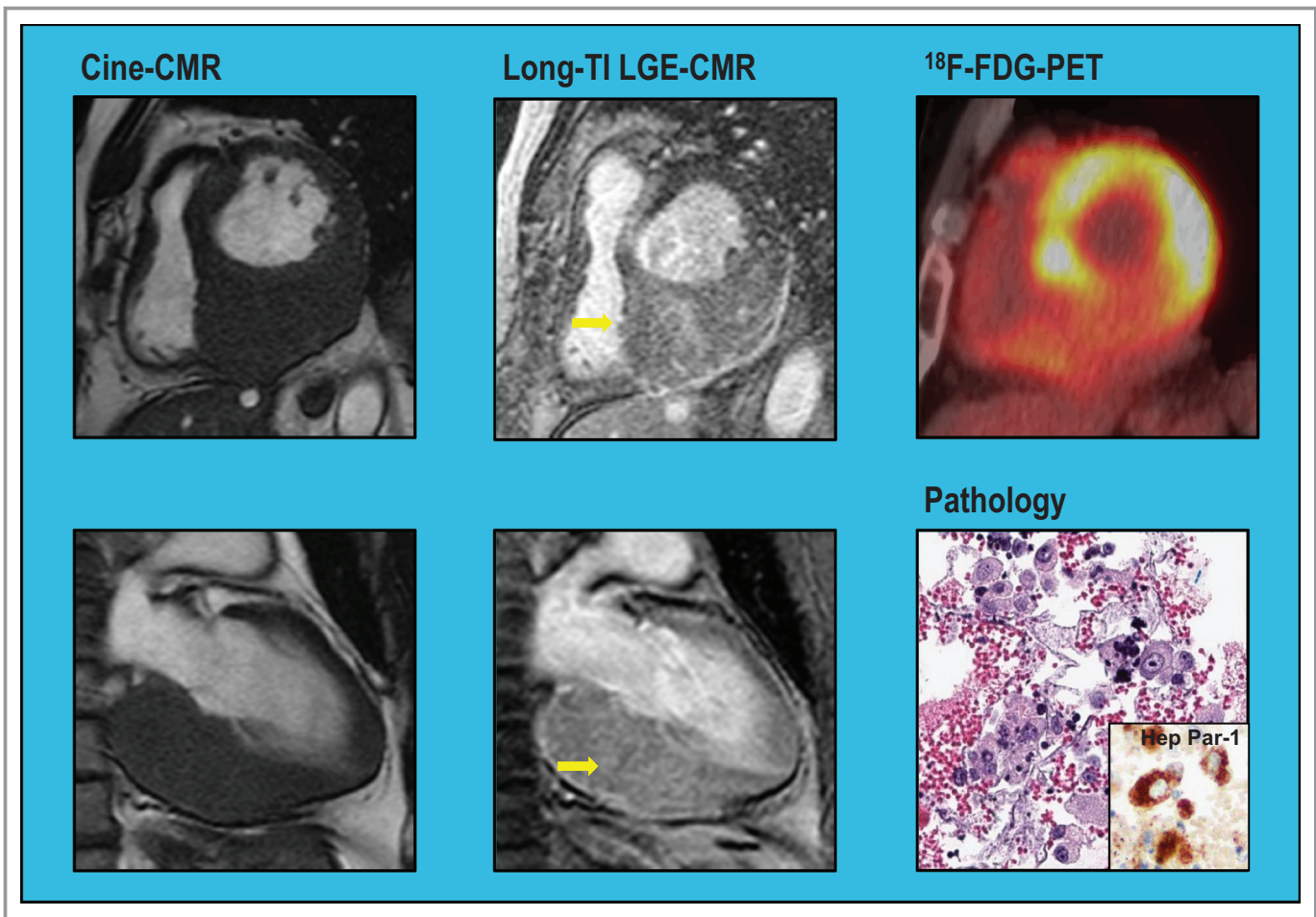
Figure 4. Differential detection of intramyocardial cardiac neoplasm. Marked asymmetric thickening of the left ventricular (LV) inferior wall in a patient with stage IV hepatocellular carcinoma. Long inversion time (long-TI) late gadolinium enhancement CMR (LGE-CMR) demonstrates contrast enhancement, consistent with NEO, whereas ^{18}F-fluorodeoxyglucose–positron emission tomography (^{18}F-FDG–PET) demonstrates low FDG avidity compared with surrounding (nonhypertrophied) LV walls. Biopsy of adjacent mediastinal lymph nodes demonstrated atypical cells (hematoxylin and eosin stain); immunostaining (anti–Hep Par 1 [hepatocyte paraffin 1] antibody) showed Hep Par 1–positive (dark brown) cells consistent with hepatocellular carcinoma. Cine-CMR indicates cine–cardiac magnetic resonance.

normalized SUV yielded higher sensitivity than did visual PET reads (70%) paralleled by higher specificity (78%).

Clinical Prognosis

Mortality was assessed after CMR and PET to test whether differential detection rates for neoplasm were accompanied by differences in prognosis. Median duration of follow-up among survivors was 1.7 years (IQR: 0.6–3.4 years); among the overall cohort (inclusive of survivors and deaths), follow-up was similar between modalities (CMR: 0.8 year [IQR: 0.4–1.9 years]; PET: 0.9 year [IQR: 0.4–1.9 years]; P=0.86).

Figure 7A provides Kaplan–Meier survival curves for patients with neoplasm and cancer-matched controls. As shown, mortality risk was significantly higher among patients with CMR-evidenced neoplasm compared with controls (hazard ratio [HR]: 1.99 [95% CI, 1.1–3.6]; P=0.03), corresponding to

higher aggregate mortality as assessed 6 months after CMR (45% versus 20%, P=0.02). Figure 7B demonstrates that among the subgroup of neoplasm cases that were visually detected by PET (70%), magnitude of adverse prognosis versus cancer-matched controls (HR: 2.12 [95% CI, 1.01–4.44]; P=0.047) was similar to that conferred by CMR. Despite this, cross-sectional risk stratification of neoplasm patients and controls based on FDG avidity demonstrated nonsignificant differences in mortality (HR: 1.56 [95% CI, 0.85–2.74]; P=0.16).

Regarding therapy, identification of neoplasms by CMR frequently prompted a change in chemotherapy/biologic regimen (89%) and less commonly prompted initiation of targeted radiotherapy (20%) or attempted surgical resection (11%) within a short (3-month) interval following imaging. For cases in which PET identified neoplasm concomitantly with CMR, rates of change in chemotherapy/biologic regimen (84%), radiation (25%), and attempted surgical resection (9%)

Table 4. PET Metabolism in Relation to Cardiac Mass Etiology on CMR

	Neoplasm (n=46)	Thrombus (n=20)	*P* Value
Maximal FDG uptake	8.2±6.5	1.8±0.5	<0.001*
Hepatic normalized	3.9±2.8	0.8±0.2	<0.001*
Blood pool normalized	4.3±3.2	1.1±0.2	<0.001*
Mean FDG uptake	4.7±2.7	1.7±0.4	<0.001*
Hepatic normalized	2.2±1.3	0.8±0.1	<0.001*
Blood pool normalized	2.9±1.6	1.2±0.2	<0.001*
Background			
Hepatic	2.2±0.4	2.3±0.5	0.38
Blood pool	1.7±0.4	1.5±0.3	0.09
Myocardium	4.1±4.6	5.1±5.3	0.46

For cardiac masses with nondiscernable FDG uptake, PET images were coregistered to CMR so as to place volumetric region of interest (for SUV measurement) in a location corresponding to the CMR-evidenced cardiac mass. Data are shown as mean±SD. CMR indicates cardiac magnetic resonance; FDG, fluorodeoxyglucose; PET, positron emission tomography; SUV, standardized uptake value.
*denotes significant p values (< 0.05).

were of similar frequency. Of note, both groups had similar extents of extracardiac tumor involvement as assessed based on whole-body PET (3.4±2.1 versus 3.3±2.0 organ systems involved, *P*=0.85).

Discussion

This study is the first to test LGE-CMR tissue characterization of cardiac masses in relation to metabolic activity on PET. Key findings are as follows. First, among a broad cancer cohort, identification of CMR-evidenced cardiac masses by PET varied in relation to mobility and avascular tissue composition. Whereas visual PET analysis identified two thirds of CMR-evidenced neoplasm, no cases of thrombus were detected. Neoplasms undetected by PET were more likely to be highly mobile on cine-CMR than were detected lesions (*P*<0.001). Regarding neoplasm subtypes, lesions with diffuse or mixed enhancement had greater FDG uptake than did predominantly avascular lesions (*P*<0.01), paralleling higher visual PET detection rates (87% versus 63%). Quantitative analysis also demonstrated that differential detection of cardiac masses by PET paralleled lesion-specific differences in metabolic activity: Coregistration data demonstrated SUV to be 2- to 4-fold higher for neoplasm compared with thrombus (*P*<0.001). Finally, follow-up data demonstrated that modality-specific differences in neoplasm detection were accompanied by differences in prognostic risk stratification. During a median follow-up of 0.8 years (IQR: 0.4–1.9 years), mortality was higher among patients with neoplasm on CMR compared with

controls matched for cancer diagnosis and stage (HR: 1.99 [95% CI, 1.1–3.6]; *P*=0.03) despite nonsignificant differences when partitioned via FDG avidity (HR: 1.56 [95% CI, 0.85–2.74]; *P*=0.16). Among neoplasm cases detected by PET, magnitude of increased mortality risk versus matched controls (HR: 2.12 [95% CI, 1.01–4.44]; *P*=0.047) was similar to that conferred by CMR.

Regarding clinical significance, it should be recognized that this study should not be construed as a comparison between equivalent cardiac testing approaches—CMR and PET. Instead, we examined performance characteristics of PET as it is typically applied in current clinical cancer care, a setting in which whole-body PET is widely used as a primary means to assess cancer organ system involvement. Given that when PET detected a neoplasm, it yielded similar prognostic implications to LGE-CMR, our findings highlight the need for dedicated cardiac protocols when PET is used to assess patients with known or suspected cardiac metastases. Our finding that highly mobile lesions (on ECG-gated, breath-held CMR) were more likely to be undetected by whole-body PET provides a mechanistic reason for discordance between modalities, further justifying a need for tailored PET protocols (inclusive of ECG and respiratory gating) in this setting. Regarding tissue characterization, our finding that FDG-PET performance varied in relation to extent of mass-associated avascular tissue composition on LGE-CMR helps to inform clinical interpretation of seeming discordance between modalities and guide imaging strategies for assessment of tumors known to be minimally vascular and/or to contain extensive tissue necrosis. Finally, given that PET can use an array of radiotracers to assess different aspects of tumor biology, our data provide a rationale for future clinical research focused on the use of novel radiotracers to assess presence and extent of thrombus and neoplasm.

It is interesting to note that neoplasm-associated enhancement correlated with metabolic activity on FDG-PET, despite the fact that prior research has shown LGE to be a marker of myocyte necrosis.[12,13] Although the mechanism for this is uncertain, it is possible that enhancement in neoplasm reflects regions of admixed vascularity and necrosis, in which contrast permeability is increased due to impaired vascular integrity. Consistent with this, prior studies have shown that cardiac neoplasms typically demonstrate increased signal intensity on first-pass perfusion and LGE-CMR, consistent with tumor-associated vascularity and contrast retention within the extracellular space.[14,15] Even if vascular permeability is intact, contrast enhancement may reflect admixed necrotic and metabolically active tissue, for which distinction of tissue subtypes was imprecise because of limited spatial resolution of standard CMR and whole-body PET: Whereas current imaging may have been sufficient to identify large, uniformly
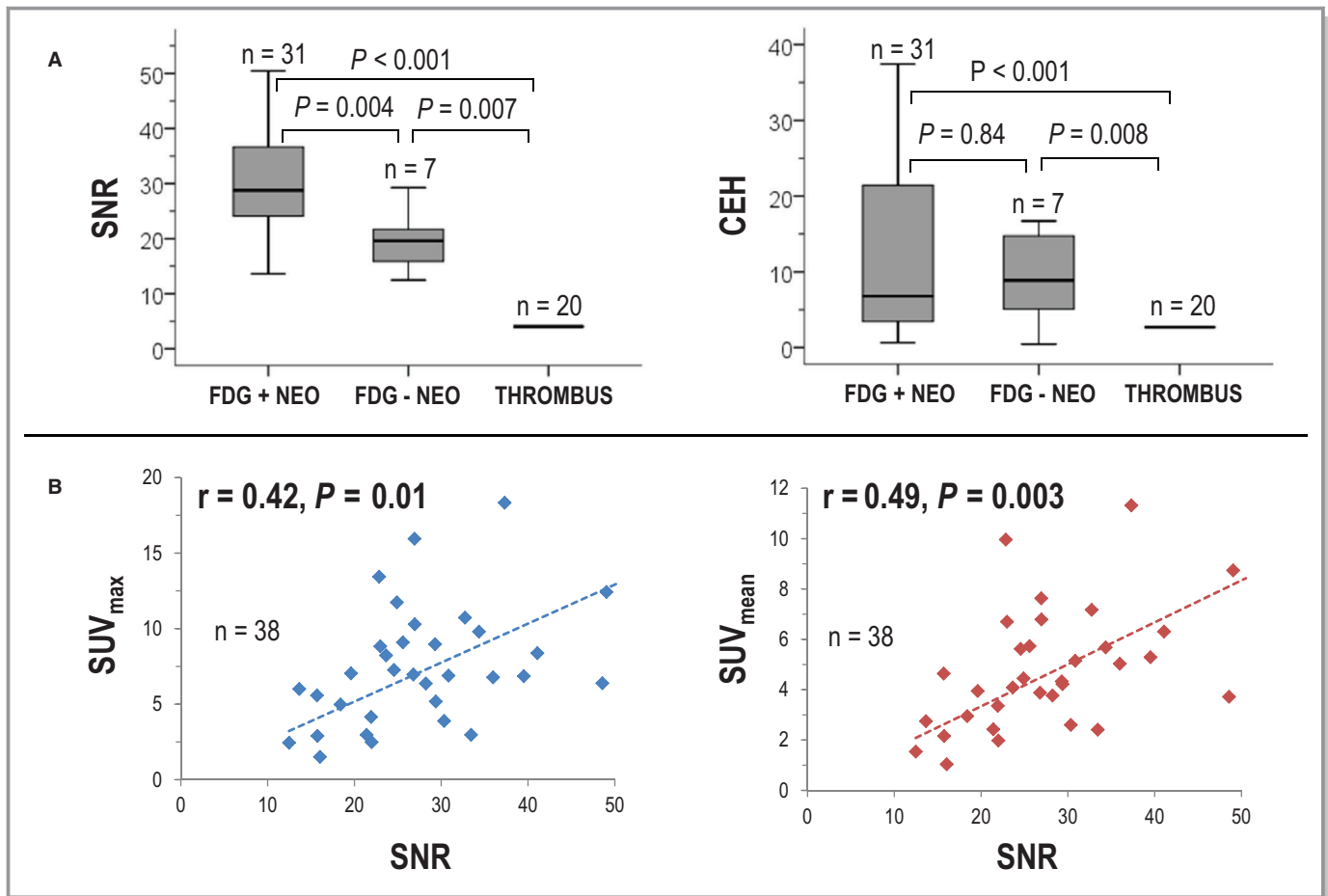
Figure 5. Quantitative contrast enhancement in relation to positron emission tomography–evidenced metabolic activity. **A**, Signal-to-noise ratio (SNR; left) and contrast-enhancement heterogeneity (CEH; right) among cardiac mass subgroups partitioned based on diagnostic test interpretation. Note higher SNR for fluorodeoxyglucose (FDG) avid vs nonavid neoplasm (NEO; *P*=0.004), paralleling higher SNR and CEH for both NEO subtypes vs thrombus (THR; both *P*<0.001). Data shown as median plus or minus interquartile range. **B**, Scatter plots demonstrating correlation between SNR and standardized uptake value (SUV) within NEO. Highly mobile lesions excluded from analyses (due to imprecise colocalization). Note significant correlations between magnitude of contrast-enhancement and FDG avidity (*P*<0.05).

avascular regions, imprecise spatial resolution and colocalization between modalities may have blunted subtle distinctions between microscopic regions of admixed enhancement and necrosis. Future studies using hybrid PET–CMR strategies are warranted to test these concepts.

Because FDG uptake is a marker of glucose metabolism,[16–18] it is not unexpected that thrombi were uniformly undetected by PET. These data support the notion that lack of enhancement on CMR is a marker of metabolically inert tissue —complementing prior data from our group and others validating absence of enhancement as a criterion for thrombus that corresponds to histopathology and stratifies embolic event risk.[1,5,10,19] Our findings regarding neoplasm subtypes expand on this concept—demonstrating that hypoenhancement corresponds to metabolically inert regions and that this finding affects differential detection between CMR and PET. Consistent with this, prior noncardiac imaging research in cancer cohorts has reported that malignant lesions can occasionally be

metabolically indolent and thus not visualized on PET.[20,21] For example, in neuroradiology studies for which diagnostic confirmation has been derived from histopathology or clinical disease progression,[22] FDG-PET has yielded sensitivity (65–86%) and specificity (80–81%) within ranges similar to our current results. Of note, novel PET tracers have been used to assess inflammation, hypoxia, and vascular supply. Given our finding that nonenhancing cardiac lesions can be inert on FDG-PET, further research is warranted to test the utility of alternative PET tracers for assessment of thrombi as well as neoplasms with extensive tumor necrosis.

To the best of our knowledge, only 2 prior case series have tested quantitative SUV cutoffs for cardiac masses. Consistent with our results, Nensa et al reported higher maximum SUV in malignant (compared with benign) lesions.[2] However, this study comprised a small number of patients (n=20), applied nonspecific morphologic criteria to distinguish between malignant and benign etiology, and included no

Table 5. PET Metabolism in Relation to Cardiac Neoplasm Enhancement Pattern on CMR

	Neoplasm Enhancement Patterns, Mean ±SD			P Value			
	Predominantly Avascular (A)	Mixed (B)	Diffuse Enhancement (C)	A-B	B-C	A-C	P Value (ANOVA)
FDG uptake							
Overall	2.3±1.2	4.7±1.9	5.9±2.5	0.005*	0.19	0.001*	0.001*
Maximal	2.6±1.2	5.8±2.7	7.1±2.8	0.005*	0.25	<0.001*	0.001*
Minimal	2.1±1.1	3.0±1.3	5.8±2.8	0.15	0.001*	<0.001*	<0.001*
Max/min	1.3±0.5	2.2±1.2	1.3±0.4	0.06	0.03*	0.92	0.007*

Excluded highly mobile neoplasm (N_A=7, N_B=10, N_C=15). Measurements derived from 2-dimensional regions of interest colocalized to areas of hyper- and hypoenhancement on CMR. CMR indicates cardiac magnetic resonance; FDG, fluorodeoxyglucose; PET, positron emission tomography.
*denotes significant p values (< 0.05).

prognostic data. In another study, Rahbar et al reported mean SUV to be higher in malignant cardiac neoplasms than in benign neoplasms.[4] Although this study partitioned groups based on histopathology, potential selection bias (requirement for pathological verification) prohibited evaluation of PET in a broad cancer cohort reflective of standard clinical
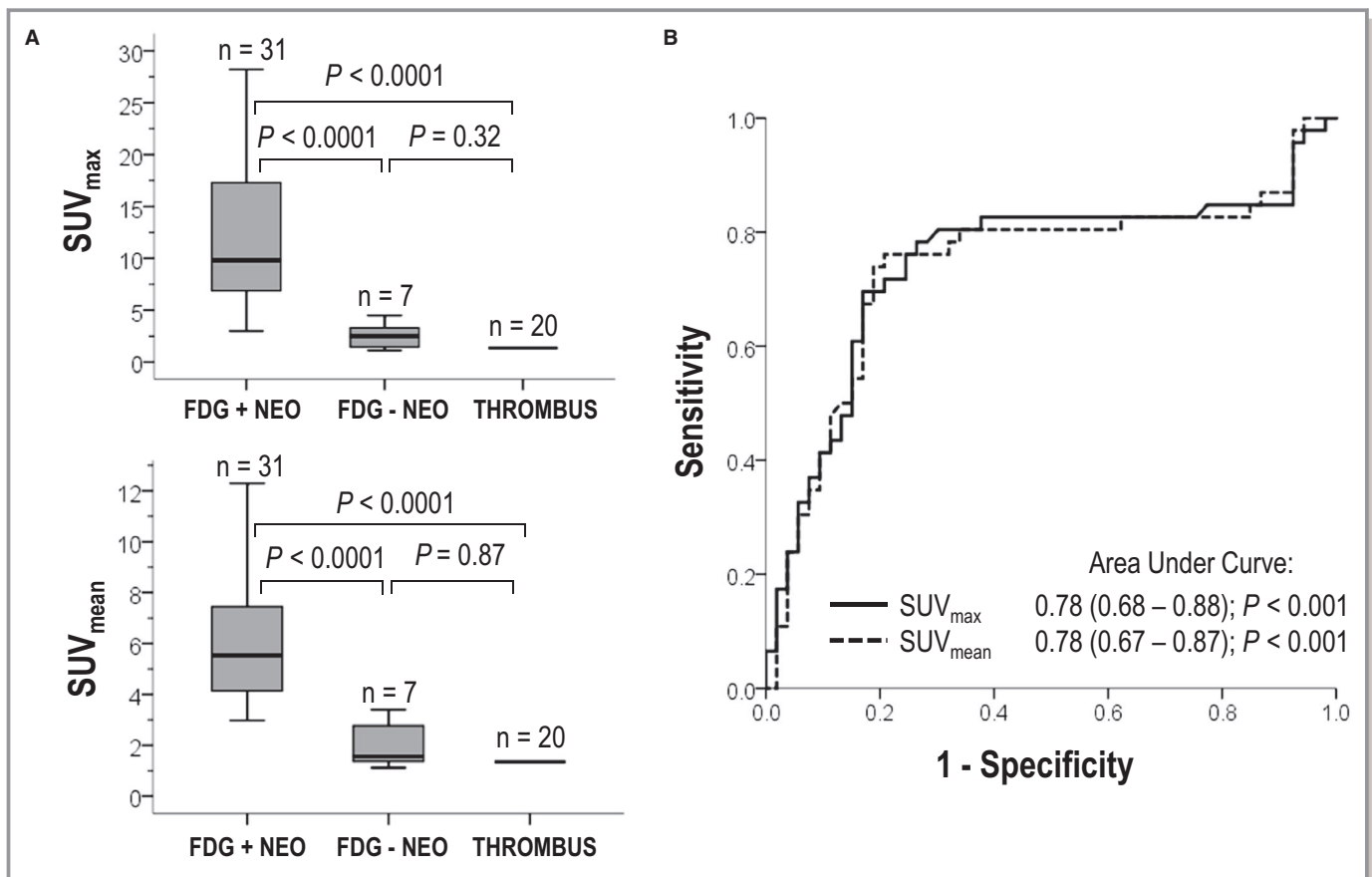
Figure 6. Quantitative metabolic activity as marker of cardiac neoplasm. **A**, Quantitative standardized uptake values (SUV) within visually scored cardiac mass subtypes. Note correspondence between visually assigned categories and quantitative results, as shown by 3- to 4-fold increment in maximum (top) and mean (bottom) quantitative SUV for neoplasm (NEO) cases visually identified on positron emission tomography (PET) vs cases in which NEO was not visually discernable ($P<0.001$), as well as similar SUV between thrombus (THR; all PET negative) and NEO cases for which PET read discordantly with cardiac magnetic resonance (CMR; $P=0.87$ and $P=0.32$ for maximum and mean SUVs, respectively). **B**, Receiver operating characteristic (ROC) curves for maximum and mean SUV cutoffs in relation to late gadolinium enhancement CMR evidenced NEO. Note good overall diagnostic performance for quantitative SUV (area under the curve: 0.78); corresponding diagnostic test parameters as derived from ROC curves shown in Table 4.

Table 6. Diagnostic Performance of Quantitative PET for Cardiac Neoplasm on CMR

	Sensitivity	Specificity	Accuracy	Positive Predictive Value	Negative Predictive Value
Signal intensity variables					
SUV_{max}	70% (32/46)	88% (66/75)	81% (98/121)	76% (35/46)	85% (64/75)
SUV_{mean}	74% (34/46)	87% (65/75)	82% (99/121)	77% (34/44)	84% (65/77)
Hepatic normalized SUV					
SUV_{max}	83% (38/46)	84% (63/75)	83% (101/121)	76% (38/50)	89% (63/71)
SUV_{mean}	80% (37/46)	84% (63/75)	82% (100/121)	76% (37/49)	88% (63/72)
Blood pool normalized SUV					
SUV_{max}	76% (35/46)	85% (64/75)	82% (99/121)	76% (35/46)	85% (64/75)
SUV_{mean}	78% (36/46)	83% (62/75)	81% (98/121)	73% (36/49)	86% (62/72)

Data are shown as percentage (frequency). CMR indicates cardiac magnetic resonance; FDG, fluorodeoxyglucose; max, maximum; PET, positron emission tomography; SUV, standardized uptake value.

Cutoffs derived (for maximum sensitivity and specificity) from receiver operating characteristic curves shown in Figure 6 (parameter-based cutoffs as follows; SUV_{max} 4.44, SUV_{mean} 2.89, hepatic normalized SUV_{max} 1.05, hepatic normalized SUV_{mean} 1.06, blood pool normalized SUV_{max} 1.78, blood pool normalized SUV_{mean} 1.35).

practice. Other information concerning quantitative SUV data in patients with neoplasm is derived from case reports, several of which reported values consistent with our results.[23–26] Although these data indicate that our findings are concordant with established literature, we are unaware of prior studies that have shown quantitative SUV cutoffs to provide incremental utility for detection of neoplasm established by LGE-CMR.
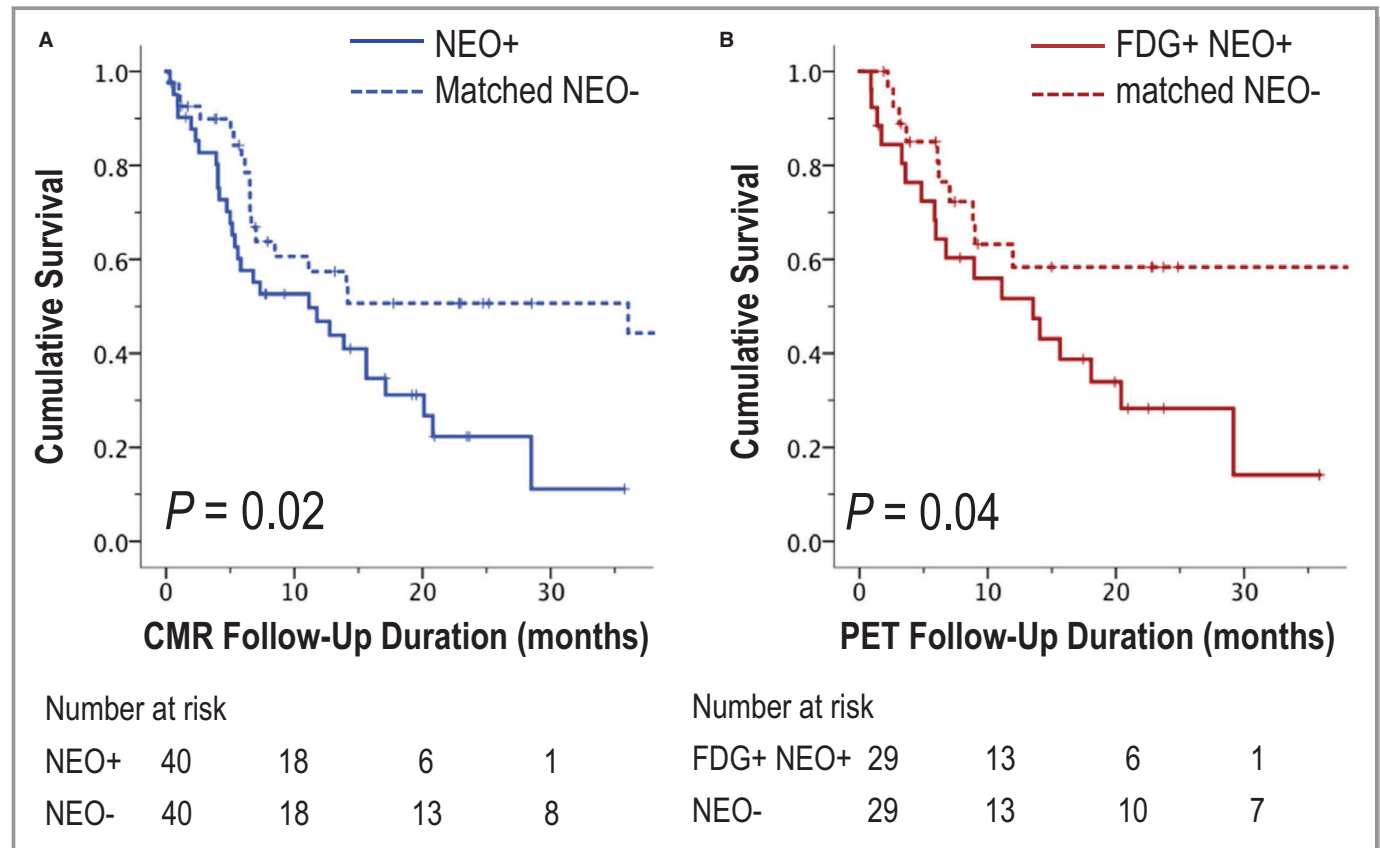
Figure 7. Mortality status. **A**, Kaplan–Meier survival curves for cardiac magnetic resonance (CMR)–evidenced neoplasm (NEO; solid line) and cancer-matched controls (dotted line). Note increased mortality among patients with NEO compared with controls matched for primary cancer type and stage (*P*=0.02). **B**, Corresponding Kaplan–Meier curves for fluorodeoxyglucose (FDG)–avid NEO and matched controls demonstrates a similar relationship (*P*=0.04). PET indicates positron emission tomography.

Several limitations should be noted. First, our study entailed analysis of preexisting imaging data, for which posttest referral (or other sources of) bias could have affected decisions to refer for PET or CMR and thus affected research results. Whereas our study provides important insights regarding current practice patterns in cardio-oncology, findings warrant further confirmation in future prospective studies. It should also be noted that while diagnostic performance of PET did not substantially vary when stratified by median interval between tests (14.8 days), it is possible that antineoplastic therapies given in the time period between PET and CMR could have resulted in discrepancies between tests. For example, given our finding that avascular masses were less likely to be discerned by FDG-PET, it is possible that tumor activity (ie, cell proliferation in excess of vascular supply) could have induced tissue necrosis and that tissue necrosis could be further affected by antineoplastic therapies administered in the interval between CMR and whole-body PET. In addition, our population was accrued at a single tertiary-care cancer center; cardiac mass–affected cases and controls were matched for cancer etiology and stage to test prognostic implications of CMR- and PET-evidenced tissue characterization. In this context, mortality rates may not reflect those of a general cancer population with a given diagnosis. Finally, test performance of quantitative PET (SUV) was assessed using cutoff values chosen from the same data rather than separate derivation and validation cohorts. Although cutoffs in our study are consistent with those of prior studies, results may be optimistic and should be tested in larger scale independent cohorts.

In conclusion, findings of this study demonstrate that among cancer patients with cardiac masses, the presence and magnitude of contrast enhancement on LGE-CMR parallels FDG metabolic activity on PET. Whereas contrast-enhancing and FDG-avid cardiac lesions portend similarly poor prognosis, augmented neoplasm detection of avascular and/or highly mobile neoplasms by CMR results in improved prognostic risk stratification. Future research is warranted to establish cellular mechanisms of contrast enhancement in FDG-avid regions and to test the utility of enhancement pattern as a marker of prognosis and therapeutic response among patients with cardiac neoplasms.

Sources of Funding

Disclosures

None.

References

1. Chan AT, Plodkowski AJ, Pun SC, Lakhman Y, Halpenny DF, Kim J, Goldburg SR, Matasar MJ, Moskowitz CS, Gupta D, Steingart R, Weinsaft JW. Prognostic utility of differential tissue characterization of cardiac neoplasm and thrombus via late gadolinium enhancement cardiovascular magnetic resonance among patients with advanced systemic cancer. *J Cardiovasc Magn Reson*. 2017;19:76.

2. Nensa F, Tezgah E, Poeppel TD, Jensen CJ, Schelhorn J, Kohler J, Heusch P, Bruder O, Schlosser T, Nassenstein K. Integrated ^{18}F-FDG PET/MR imaging in the assessment of cardiac masses: a pilot study. *J Nucl Med*. 2015;56:255–260.

3. Pun SC, Plodkowski A, Matasar MJ, Lakhman Y, Halpenny DF, Gupta D, Moskowitz C, Kim J, Steingart R, Weinsaft JW. Pattern and prognostic implications of cardiac metastases among patients with advanced systemic cancer assessed with cardiac magnetic resonance imaging. *J Am Heart Assoc*. 2016;5:e003368. DOI: 10.1161/JAHA.116.003368.

4. Rahbar K, Seifarth H, Schafers M, Stegger L, Hoffmeier A, Spieker T, Tiemann K, Maintz D, Scheld HH, Schober O, Weckesser M. Differentiation of malignant and benign cardiac tumors using ^{18}F-FDG PET/CT. *J Nucl Med*. 2012;53:856–863.

5. Srichai MB, Junor C, Rodriguez LL, Stillman AE, Grimm RA, Lieber ML, Weaver JA, Smedira NG, White RD. Clinical, imaging, and pathological characteristics of left ventricular thrombus: a comparison of contrast-enhanced magnetic resonance imaging, transthoracic echocardiography, and transesophageal echocardiography with surgical or pathological validation. *Am Heart J*. 2006;152:75–84.

6. Weinsaft JW, Kim HW, Crowley AL, Klem I, Shenoy C, Van Assche L, Brosnan R, Shah DJ, Velazquez EJ, Parker M, Judd RM, Kim RJ. LV thrombus detection by routine echocardiography: insights into performance characteristics using delayed enhancement CMR. *JACC Cardiovasc Imaging*. 2011;4:702–712.

7. Weinsaft JW, Kim HW, Shah DJ, Klem I, Crowley AL, Brosnan R, James OG, Patel MR, Heitner J, Parker M, Velazquez EJ, Steenbergen C, Judd RM, Kim RJ. Detection of left ventricular thrombus by delayed-enhancement cardiovascular magnetic resonance prevalence and markers in patients with systolic dysfunction. *J Am Coll Cardiol*. 2008;52:148–157.

8. Weinsaft JW, Kim RJ, Ross M, Krauser D, Manoushagian S, LaBounty TM, Cham MD, Min JK, Healy K, Wang Y, Parker M, Roman MJ, Devereux RB. Contrast-enhanced anatomic imaging as compared to contrast-enhanced tissue characterization for detection of left ventricular thrombus. *JACC Cardiovasc Imaging*. 2009;2:969–979.

9. Fussen S, De Boeck BWL, Zellweger MJ, Bremerich J, Goetschalckx K, Zuber M, Buser PT. Cardiovascular magnetic resonance imaging for diagnosis and clinical management of suspected cardiac masses and tumours. *Eur Heart J*. 2011;32:1551–1560.

10. Goyal P, Weinsaft JW. Cardiovascular magnetic resonance imaging for assessment of cardiac thrombus. *Methodist Debakey Cardiovasc J*. 2013;9:132–136.

11. Bussani R, De-Giorgio F, Abbate A, Silvestri F. Cardiac metastases. *J Clin Pathol*. 2007;60:27–34.

12. Kim RJ, Fieno DS, Parrish TB, Harris K, Chen EL, Simonetti O, Bundy J, Finn JP, Klocke FJ, Judd RM. Relationship of MRI delayed contrast enhancement to irreversible injury, infarct age, and contractile function. *Circulation*. 1999;100:1992–2002.

13. Fieno DS, Kim RJ, Chen EL, Lomasney JW, Klocke FJ, Judd RM. Contrast-enhanced magnetic resonance imaging of myocardium at risk: distinction between reversible and irreversible injury throughout infarct healing. *J Am Coll Cardiol*. 2000;36:1985–1991.

14. Beroukhim RS, Prakash A, Valsangiacomo Buechel ER, Cava JR, Dorfman AL, Festa P, Hlavacek AM, Johnson TR, Keller MS, Krishnamurthy R, Misra N, Moniotte S, Parks WJ, Powell AJ, Soriano BD, Srichai MB, Yoo S-J, Zhou J, Geva T. Characterization of cardiac tumors in children by cardiovascular magnetic resonance imaging. *J Am Coll Cardiol*. 2011;58:1044.

15. Pazos-Lopez P, Pozo E, Siqueira ME, Garcia-Lunar I, Cham M, Jacobi A, Macaluso F, Fuster V, Narula J, Sanz J. Value of CMR for the differential diagnosis of cardiac masses. *JACC Cardiovasc Imaging*. 2014;7:896–905.

16. Kelloff GJ, Hoffman JM, Johnson B, Scher HI, Siegel BA, Cheng EY, Cheson BD, O'Shaughnessy J, Guyton KZ, Mankoff DA, Shankar L, Larson SM, Sigman CC, Schilsky RL, Sullivan DC. Progress and promise of FDG-PET imaging for cancer patient management and oncologic drug development. *Clin Cancer Res*. 2005;11:2785–2808.

17. Plathow C, Weber WA. Tumor cell metabolism imaging. *J Nucl Med*. 2008;49 (suppl 2):43s–63s.

18. Vander Heiden MG, Cantley LC, Thompson CB. Understanding the Warburg effect: the metabolic requirements of cell proliferation. *Science*. 2009;324:1029–1033.

19. Poss J, Desch S, Eitel C, de Waha S, Thiele H, Eitel I. Left ventricular thrombus formation after ST-segment-elevation myocardial infarction: insights from a cardiac magnetic resonance multicenter study. *Circ Cardiovasc Imaging*. 2015;8:e003417.

20. Karam M, Novak L, Cyriac J, Ali A, Nazeer T, Nugent F. Role of fluorine-18 fluoro-deoxyglucose positron emission tomography scan in the evaluation and follow-up of patients with low-grade lymphomas. *Cancer*. 2006;107: 175–183.

21. Beiderwellen K, Gomez B, Buchbender C, Hartung V, Poeppel TD, Nensa F, Kuehl H, Bockisch A, Lauenstein TC. Depiction and characterization of liver lesions in whole body [18F]-FDG PET/MRI. *Eur J Radiol*. 2013;82:e669–e675.

22. Chao ST, Suh JH, Raja S, Lee SY, Barnett G. The sensitivity and specificity of FDG PET in distinguishing recurrent brain tumor from radionecrosis in patients treated with stereotactic radiosurgery. *Int J Cancer*. 2001;96:191–197.

23. Freudenberg LS, Rosenbaum SJ, Schulte-Herbruggen J, Eising EG, Lauenstein T, Wolff A, Bockisch A. Diagnosis of a cardiac angiosarcoma by fluorine-18 fluordeoxyglucose positron emission tomography. *Eur Radiol*. 2002;12(suppl 3):S158–S161.

24. Shimotsu Y, Ishida Y, Fukuchi K, Hayashida K, Toba M, Hamada S, Takamiya M, Satoh T, Nakanishi N, Nishimura T. Fluorine-18-fluorodeoxyglucose PET identification of cardiac metastasis arising from uterine cervical carcinoma. *J Nucl Med*. 1998;39:2084–2087.

25. Wenning C, Engelen MA, Rahbar K, Wenker M, Stypmann J, Spieker T, Schober O, Weckesser M, Stegger L. Therapy refractory coronary compression caused by a cardiac metastasis: the role of imaging. *J Nucl Cardiol*. 2010;17:696–698.

26. Zhang M, Li B, Jiang X. PET/CT imaging in a case of cardiac liposarcoma. *J Nucl Cardiol*. 2008;15:473–475.

SUPPLEMENTAL MATERIAL

Data S1.

Supplemental Methods

Detailed below are definitions and related methodological aspects of analyses performed for key study related imaging variables:

Signal-to-noise ratio (SNR)

  Ratio between signal intensity within a region of interest (ROI) drawn over the entire C_{MASS}, and standard deviation of signal intensity of background noise within an ROI (~100mm^2) measured on the same long-TI LGE-CMR image with largest visualized C_{MASS}.

$$SNR = \frac{Intensity_{CMASS}}{Intensity_{SD\,of\,Noise}}$$

Contrast-enhancement heterogeneity (CEH)

  Ratio of maximum and minimum signal intensity difference within a given C_{MASS}, and standard deviation of signal intensity of background noise within an ROI (~100mm^2) measured on the same long-TI LGE-CMR image with largest visualized C_{MASS}.

$$CEH = \frac{Intensity_{Maximum\,signal\,within\,CMASS} - Intensity_{Minimum\,signal\,within\,CMASS}}{Intensity_{SD\,of\,Noise}}$$

Maximum and mean standardized uptake unit (SUV$_{max}$, SUV$_{mean}$)

  SUV$_{max}$ and SUV$_{mean}$ refer to maximum and mean FDG intensities as measured on PET within an ROI placed over the entire C_{MASS}.

  To examine differences in regional (mean) SUV uptake among cardiac neoplasms grouped based on pattern of late gadolinium enhancement (predominantly avascular, mixed, and diffuse enhancement),

two ROIs were drawn on the C_{MASS} corresponding to areas with maximum and minimum signal intensities on a PET image co-registered to long-TI LGE-CMR (data reported in **Table 3B**).

To examine correlations between SNR (on long-TI LGE-CMR) and SUV (on PET), SUV_{max} and SUV_{mean} were tested in relation to SNR as measured (using the above referenced methods) on co-registered PET and long TI LGE-CMR images (data reported in **Figure 5B**).

Supplemental Video Legends:

Video S1. Cine-CMR demonstrating mobile intra-cardiac mass partially adherent to the aortic valve as identified in through plane aortic valve (left) and LV 3-chamber long axis (right) orientations (still frame image LGE-CMR, PET, and pathology shown in Figure 3). Best viewed with Windows Media Player.

Video S2. Cine-CMR demonstrating marked asymmetric thickening of the LV inferior wall as identified in LV short axis (left) and 2-chamber long axis (right) orientations (still frame image LGE-CMR, PET, and pathology shown in Figure 4). Best viewed with Windows Media Player.